Digital quantification of Ki67 and PRAME in challenging melanocytic lesions - A novel diagnostic tool

Brogård, Mette Bak; Steiniche, Torben; Lade-Keller, Johanne; Wandler, Anne; Christensen, Kristina Bang; Georgsen, Jeanette Bæhr; Nielsen, Patricia Switten

Published in:
Pathology Research and Practice

DOI (link to publication from Publisher):
10.1016/j.prp.2025.155953

Publication date:
2025

Document Version
Publisher's PDF, also known as Version of record

Pathology - Research and Practice 270 (2025) 155953

Contents lists available at ScienceDirect

Pathology - Research and Practice

journal homepage: www.elsevier.com/locate/prp

Digital quantification of Ki67 and PRAME in challenging melanocytic lesions – A novel diagnostic tool

Mette Bak Brogård [a,b,*], Torben Steiniche [a,b], Johanne Lade-Keller [c], Anne Wandler [a], Kristina Bang Christensen [a], Jeanette Bæhr Georgsen [a,b], Patricia Switten Nielsen [a,b]

[a] Department of Pathology, Aarhus University Hospital, Palle Juul-Jensens Boulevard 35, 8200 Aarhus, Denmark
[b] Department of Clinical Medicine, Aarhus University, Palle Juul-Jensens Boulevard 99, 8200 Aarhus, Denmark
[c] Department of Pathology, Aalborg University Hospital, Ladegårdsgade 3, 9000 Aalborg, Denmark

ARTICLE INFO

Keywords:
Melanocytic lesions
Ki67
PRAME
MPATH-Dx classification
Digital pathology
Artificial intelligence
Multiplex immunohistochemistry

ABSTRACT

The interpretation of immunohistochemical markers in melanocytic lesions possesses difficulties due to expression in non-melanocytic cells and the time-consuming, non-reproducible nature of manual assessment. A digital tool that accurately quantifies Ki67 and PRAME may valuably aid pathologists in the diagnostic classification of melanocytic lesions. The aim of this study was to assess the diagnostic performance of digitally quantified Ki67 and PRAME in challenging melanocytic lesions utilizing double nuclear staining methods for accurate identification of melanocytic cells. We explored the difference in Ki67 and PRAME expression by WHO-lesion-groups and Melanocytic Pathology Assessment Tool and Hierarchy for Diagnosis version 2.0 (MPATH-Dx V2.0). Tissue slides from a cohort of 156 melanocytic lesions were stained with the Ki67/SOX10 double nuclear stain and the PRAME/SOX10 virtual double nuclear stain. Melanocytic cell specific Ki67/SOX10- and PRAME/SOX10-indexes were quantified by AI-driven digital image analysis (DIA) and compared to non-specific Ki67- and PRAME-indexes. The results showed that ROC AUC of the Ki67/SOX10-index was increased compared to the non-specific Ki67-index ($p < 0.001$), as opposed to the AUC of the PRAME/SOX10-index compared to non-specific PRAME-index ($p = 0.090$). The medians of digitally quantified Ki67- and PRAME-indexes differed significantly for the overall WHO-groups and MPATH-Dx V2.0 classes ($p < 0.001$). In conclusion, we found that double nuclear staining improved the diagnostic performance of Ki67, but not PRAME. The combination of digitally quantified Ki67- and PRAME-indexes may potentially serve as a tool for diagnostic classification of challenging melanocytic lesions. The proposed diagnostic tool presents the results visually, graphically, and quantitatively to optimally aid the pathologist.

1. Introduction

An accurate diagnosis of melanoma is essential to ensure the patients the best possible treatment and prognosis[1–3]. Unfortunately, the diagnostic assessment of melanocytic lesions can sometimes be very challenging, even for experienced dermatopathologists[4].

The histological diagnosis relies on specific morphological features characteristic of melanoma, however, some of these features can also appear in non-malignant lesions[5,6]. The diagnostic evaluation is particularly challenging when assessing, for example, atypical or dysplastic nevi or various forms of Spitz nevi[2,4]. Previously, the clinical diagnosis has primarily focussed on classifying melanocytic lesions as either benign or malignant. More recently, the World Health Organization (WHO) has added an intermediate group including dysplastic lesions, melanoma in situ, and the so-called melanocytomas, to acknowledge the varying risk of progression associated with lesions in these groups[7]. Additionally, a new management-based classification system has been proposed; the Melanocytic Pathology Assessment Tool and Hierarchy for Diagnosis (MPATH-Dx)[8]. The updated MPATH-Dx version 2.0 comprises four classes that aim to standardize the diagnostic report in relation to the clinical treatment[2]. As an example, re-resection is recommended for MPATH-Dx V2.0 class II lesions with positive margins, while this is not required for class I lesions[2]. Accordingly, the need for objective diagnostic tools to aid the histopathological assessment and ensure accurate and reproduceable diagnostic classification cannot be overstated, especially for challenging

* Corresponding author at: Department of Pathology, Aarhus University Hospital, Palle Juul-Jensens Boulevard 35, Aarhus 8200, Denmark.
E-mail addresses: mettbrog@clin.au.dk, mettbrog@rm.dk (M.B. Brogård).

https://doi.org/10.1016/j.prp.2025.155953
Received 18 December 2024; Received in revised form 6 March 2025; Accepted 28 March 2025
Available online 31 March 2025

melanocytic lesions[2,4].

Nowadays, pathologists often utilize immunohistochemical (IHC) stains as a diagnostic aid in the assessment of challenging melanocytic lesions. The toolbox includes various IHC-markers, both markers of melanocytic cells as S100, SOX10, or MART1, and markers that indicate possible malignancy, such as high Ki67, no HMB45 loss in dermal parts, or positivity of the newly proposed IHC marker PRAME (PReferentially expressed Antigen in MElanoma)[9–12]. However, none of these markers alone have been able to fully distinguish between benign and malignant lesions[6]. Furthermore, the difficulty and lack of standardization in the manual interpretation of IHC markers leads to a substantial interobserver variance and a lack of reproducibility[13,14]. Implementation of standardized and observer-independent assessment methods may improve the diagnostic efficacy of IHC markers[15–18]. The utilization of automated digital quantification and artificial intelligence to assess IHC stains could potentially solve this task.

In this study, we focus on two of the most widely used IHC markers in melanoma diagnosis: Ki67 and PRAME[11,19]. Previous research has demonstrated their superior diagnostic performance compared to the marker HMB45[20–22]. Ki67 is a widely used marker of cell proliferation that stains nuclei in all active phases of cell-cycle proliferation (G1, S, G2, and M)[5,9,23,24]. Melanomas exhibit a relatively high proportion of Ki67 positive cells, which are distributed throughout the dermis. In contrast, Ki67 positivity is very low and located superficially in benign nevi[5,25,26]. PRAME is a tumour-associated antigen of the cancer testis antigen family[27]. Melanomas predominantly exhibit high (diffuse) PRAME expression in contrast to benign lesions, making it a relevant diagnostic biomarker for melanocytic lesions[28]. Through the integration of Ki67 and PRAME markers in a combined digital tool, we seek to optimize their diagnostic performance.

Several studies have investigated the use of digital image analysis (DIA) to quantify Ki67 and, recently, also PRAME[26,29–35]. To quantify IHC markers digitally, it is necessary to specify the specific cells to be counted. Clinically, IHC biomarker indexes, such as those for Ki67 and PRAME, are defined based on the proportion of positive melanocytic cells among all melanocytic cells within the lesions. To accomplish this by automated DIA methods, it is theoretically essential to identify all melanocytic cells accurately. This can be achieved through the utilization of a tumour-cell marker with a high sensitivity on a cellular level. MART1 and HMB45 has previously been utilized as melanocytic tumour-cell markers in combination with both Ki67 and PRAME [26,29–31,36–39]. However, HMB45 is known to be lost in parts of melanocytic lesions, consequently reducing its sensitivity on a cellular level [20]. In previous studies, researchers in our group experienced that melanomas regularly exhibited a heterogenic MART1 staining with weak or even MART1-negative areas, thereby limiting MART1's value as a precise melanocytic marker for cell-level DIA. Moreover, MART1 is known to show poor expression in some challenging types, especially desmoplastic lesions[26,29–31]. These challenges can, possibly, be improved by the utilization of SOX10 as a melanocytic marker. SOX10 is a very distinct marker of melanocytic nuclei, and it has a high sensitivity both for different subtypes of melanocytic lesions, including desmoplastic melanomas, and on a cellular level for individual melanocytic cells (homogenous stain) [19,40,41]. Furthermore, the colocalization of the nuclear marker SOX10 and other nuclear IHC markers allows for precise identification of positive melanocytic cells. This is especially important for Ki67, since the distinction between proliferative melanocytic cells and proliferative nuclei of adjacent and overlying cells such as lymphocytes or basal keratinocytes, represents a substantial challenge and remains problematic utilizing MART1 due to is cytoplasmic localization[5,42,43]. We have recently proposed the Ki67/SOX10 double nuclear stain and the PRAME/SOX10 virtual double nuclear stain for a better and more precise visualisation of melanocytic tumour cells[32,35]. Through utilization of the double nuclear stain, it is possible to identify colocalization of the target marker and the tumour-cell marker, which is optimal for digital quantification of a tumour-cell specific biomarker index.

This study aimed to assess methods for digital quantification of Ki67 and PRAME in challenging melanocytic lesions, with the purpose of developing an objective tool to support pathologists in their diagnostic assessment and classification. To do this we 1) developed an AI-based DIA method for digital quantification of Ki67 and PRAME, 2) compared Ki67-indexes quantified by Ki67/SOX10 double nuclear stains, Ki67/MART1 double stains, or by Ki67 alone, across various tumour regions, 3) compared PRAME-indexes quantified by PRAME/SOX10 virtual double nuclear stains or by PRAME alone, across various tumour regions, 4) assessed the distribution of digitally quantified Ki67 and PRAME in WHO-groups and MPATH-Dx V2.0 classes, and 5) integrated the digitally quantified Ki67 and PRAME-indexes into a combined diagnostic tool.

2. Material and methods

2.1. Material

This study was conducted on a subset of a larger consecutive cohort of melanocytic lesions, specifically narrowed down to emphasize challenging lesions and rare subtypes (N = 156) (Fig. 1). The original consecutive cohort comprised all melanocytic lesions excised at the Department of Plastic Surgery, Aarhus University Hospital, Aarhus, Denmark, between September 2010 and February 2011. A total of 379 lesions were included, all of which were referred to the Department of Pathology at Aarhus University Hospital for evaluation of a potential melanoma. The initial clinical diagnosis of all the lesions was re-evaluated by two experienced dermatopathologist and a consensus diagnosis was established[30]. The present study cohort included all lesions of rare benign or malignant subtypes and all intermediate lesions (dysplastic lesions and melanoma in situ) from the initial consecutive cohort. The malignant group and the benign group were then supplemented with consecutively included common benign nevi and malignant lesions from the original cohort to reach approximately 50 lesions in each group as shown in Fig. 1. Following 10 years of follow up, a review of recurrence or metastases was conducted off all cases within the national pathology register. The study was approved by the Regional Committees on Health Research Ethics of the Central Denmark Region (reference number 1–10–72–317–20, initial approved 5th February 2021, updated approval 8th April 2024).

2.2. Immunohistochemistry

2.2.1. Workflow

Immunohistochemical stains of the proposed methods were performed as visualized in Fig. 2 and Suppl. Fig. 1, which also displays the proposed integrated workflow from routine digital haematoxylin-eosin (HE) (Step A), through double nuclear staining (Step B), and digital image analysis (Step C) to final presentation to the pathologist (Step D). Initially, formalin fixed, paraffin embedded (FFPE) tissue slides were stained with routine HE (HE600, Ventana Medical Systems, Inc., Tucson, AZ, USA), scanned, and displayed digitally to the pathologist (Fig. 2, Step A). An experienced dermatopathologist (JKL) outlined the overall tumour region on the scanned HE stain, which served as the focus for subsequent analysis in this study. Within the suggested workflow, the pathologist would then request Ki67 and PRAME IHC stains, performed as outlined below (Fig. 2, Step B and Suppl. Fig. 1, Step B).

2.3. Ki67/SOX10 double nuclear stain by multiplex chromogenic immunohistochemistry (mIHC)

The mIHC Ki67/SOX10 double nuclear stain was performed as visualised in Fig. 2, Step B, and described in detail in a previous published paper[32]. Briefly, the initial HE-stained tissue glasses were retrieved, and the cover glasses removed by heat (190°C). The slides

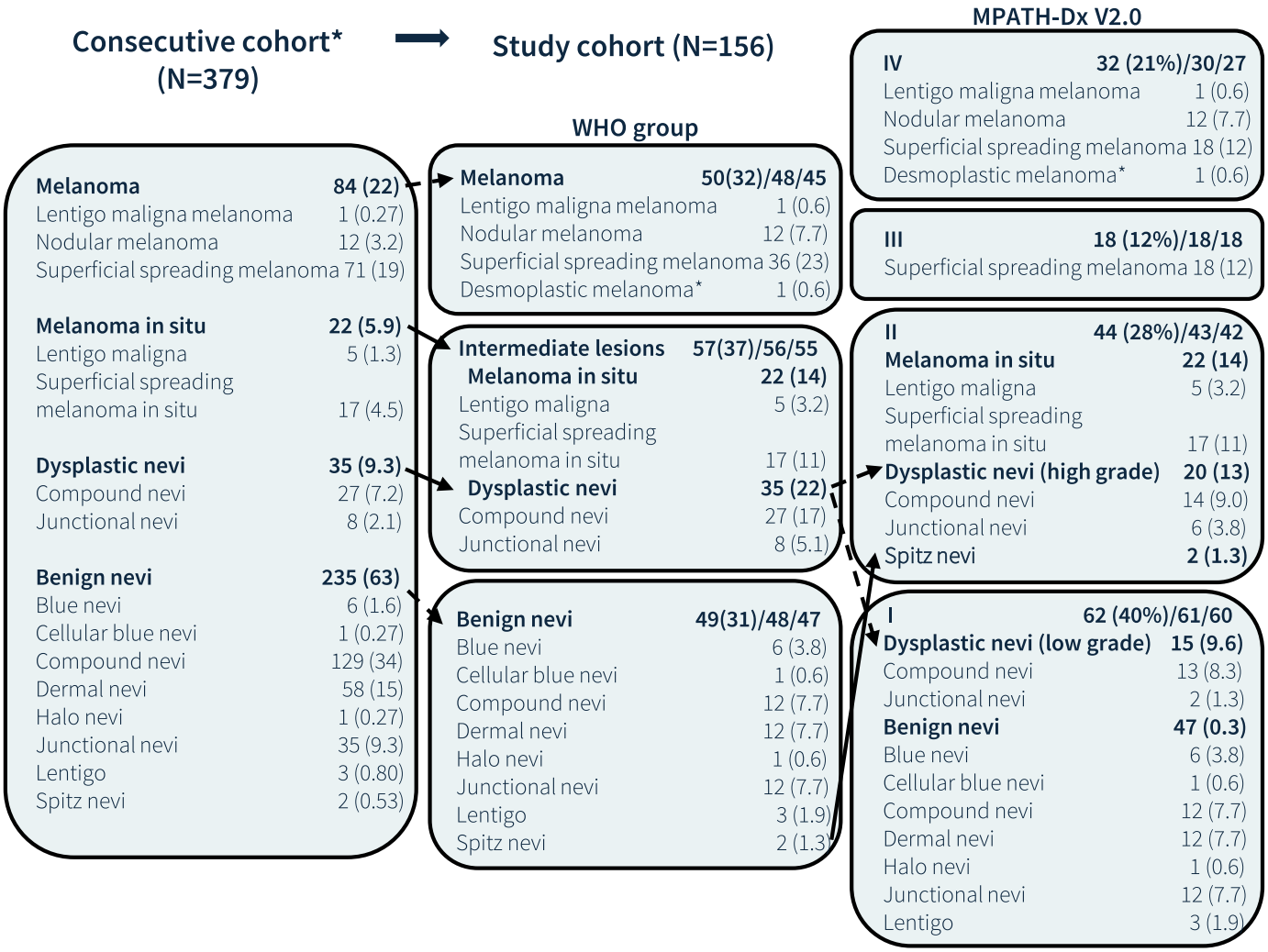

Fig. 1. Description of the study cohort, that is a subset of a larger consecutive cohort of melanocytic lesions from a previous study by Nielsen et al. 2014 (marked with *). The present study cohort included all lesions of rare benign or malignant subtypes and all intermediate lesions from the initial consecutive cohort. The malignant group and the benign group were then supplemented with consecutively included common benign nevi and malignant lesions from the original cohort to reach approximately 50 lesions in each group. Additional to the WHO-groups, the lesions included in the study cohort were classified in MPATH Dx V2.0 classes.

were then re-stained with the mIHC Ki67/SOX10 double nuclear stain (Ki67: monoclonal rabbit, clone 30–9, ready-to-use, Ventana, SOX10: monoclonal rabbit, clone SP267, ready-to-use, Ventana) performed on Ventana Discovery Ultra (Ventana) using teal chromogen for Ki67 (DISCOVERY Teal HRP kit, Ventana) and purple chromogen for SOX10 (DISCOVERY Purple HRP kit, Ventana) and standard settings and reagent kits without counterstaining and finally re-scanned. Initially, the Ki67/SOX10 double nuclear staining was performed on 3 μm slides that had been cut in 2012 and stored at −80°C. The tissue slides were reheated at 4°C and room temperature before staining. If staining of old freezer slides failed, new stains were performed on fresh cut slides from FFPE tissue blocks.

2.4. PRAME/SOX10 double nuclear stain by multiplex immunohistochemical consecutive staining on single slide (MICSSS)

The MICSSS PRAME/SOX10 double nuclear stain was performed as visualised in Suppl. Fig. 1 and described in detail in a previous published paper[35]. Briefly, fresh cut 3 μm FFPE slides for IHC were stained with primary PRAME antibody (monoclonal rabbit, clone EPR20330, dilution 1:100, Biocare Medical, Pacheco, CA, USA) using a visualization system with FastRed as the chromogen (ultraView Universal Alkaline Phosphatase Red Detection Kit, Ventana) and counterstained with haematoxylin as in routine settings. The slides where then scanned digitally and the cover glasses removed by acetone and xylene, rehydrated, and incubated in citrate-based buffer (pH 6.5). The FastRed stain was not subjected to destaining. Then slides were re-stained with primary SOX10 antibody (monoclonal rabbit, clone SP267, ready-to-use, Ventana) using a visualization system with DAB as the chromogen (OptiView DAB IHC Detection Kit, Ventana) and counterstained with haematoxylin, and re-scanned. The stains were performed on Benchmark Ultra (Ventana) using standard settings and reagent kits.

2.5. Image requisition

All stains were scanned as whole slide brightfield images at 40X magnification using Nanozoomer 2.0 HT (Hamamatsu Photonics K.K., Hamamatsu City, Japan).

2.6. Digital image analysis

2.6.1. Workflow

DIA was performed using Visiopharm Integrator System 2020.08.2.8800 including the AI architect module (Visiopharm A/S, Hoersholm, Denmark). The DIA workflow is composed of three main steps: 1) image alignment, 2) region outlining, 3) nuclei identification

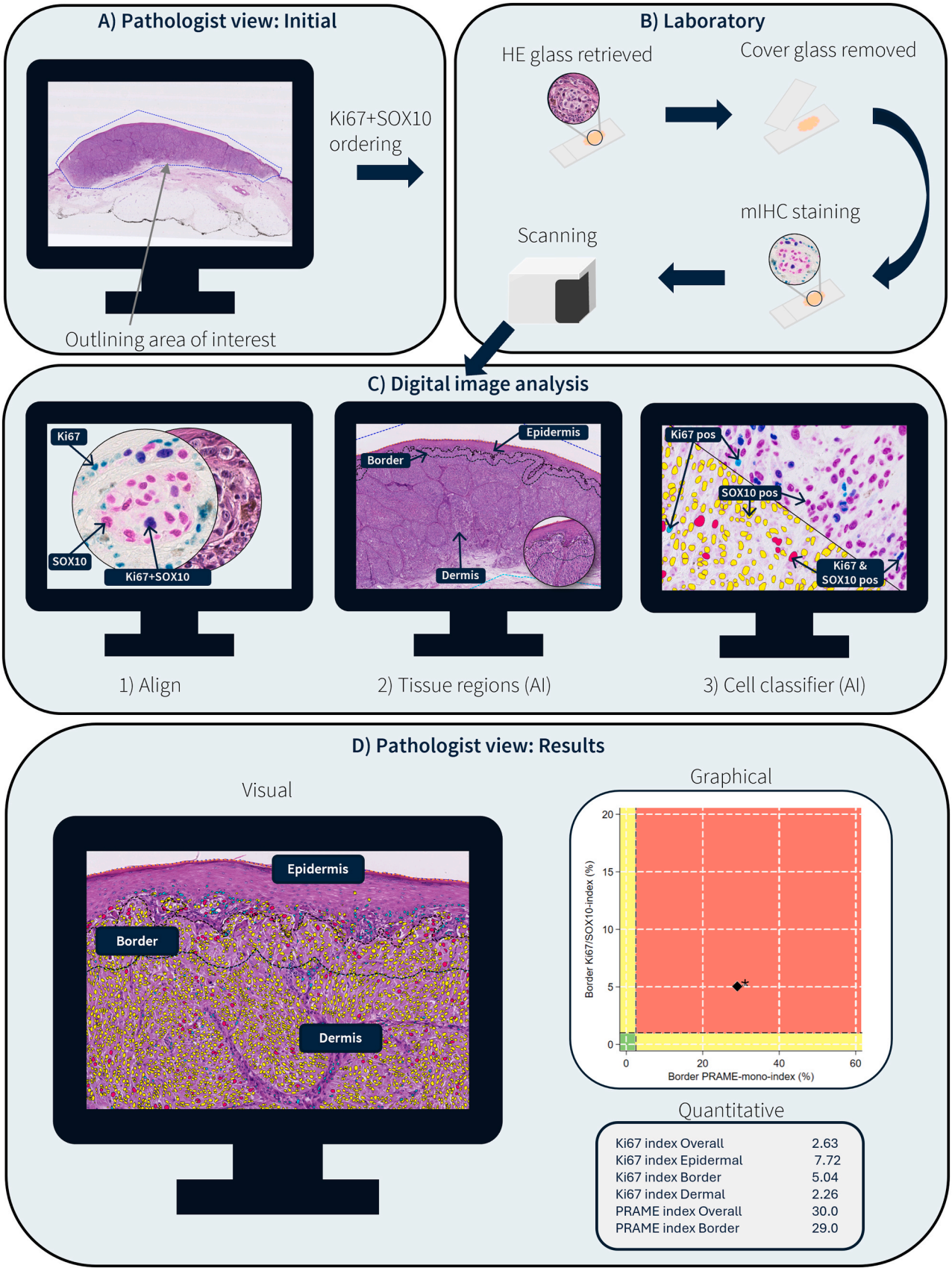

(caption on next page)

Fig. 2. Overview of the integrated workflow from routine digital haematoxylin-eosin (HE) (Step A), through double nuclear staining (Step B) and digital image analysis (Step C) to final presentation to the pathologist (Step D). In step A, the pathologist receives the digital HE stain as in routine settings at a digitalized department. When needed, the pathologist then requests additional Ki67 and PRAME immunohistochemical (IHC) stains and outlines the tumour region of interest on the digital HE image. In step B, the IHC stains are performed, here exemplified by the Ki67/SOX10 stain, that is performed on the same tissue slide initially stained with HE. The cover glass is removed and the tissue re-stained with mIHC Ki67/SOX10 and re-scanned. In step C the digital scans of the HE and mIHC stains are aligned digitally (Step 1), followed by an app identifying the epidermal border and outlining the epidermal, border and dermal tumour regions (Step 2). Next, an AI-based digital image analysis (DIA) application identifies all nuclei on the mIHC stain and classifies them according to their colour as Ki67/SOX10 double-positive (red), SOX10 mono-positive (yellow), or Ki67 mono-positive (light blue) (Step 3). Finally, in Step D, the result of the DIA is displayed to the pathologist visually, graphically, and quantitative.

and classification (Fig. 2, Step C). Additionally, hot spot analysis was performed. The Ki67- and PRAME-indexes were quantified for both the overall tumour region defined by the pathologist as well as for the different compartments: an epidermal region, a dermo-epidermal border region encountering the uppermost 100 μm of dermis including epidermal melanocytic nest, a dermal region, and a hot spot region.

2.6.2. Ki67/SOX10 digital image analysis

The two digital scans of the subsequent stains of HE and Ki67/SOX10 mIHC performed on the same tissue slide were aligned automatically using Visiopharm's Tissuealign™ (Fig. 2, Step C1). In Step C2, the overall tumour region initially outlined by the pathologist was divided in epidermis and dermis by an AI-based application (app) that automatically outlined the dermo-epidermal boundary (Suppl. Fig. 2). This app was based on a convolutional neural network (DeepLabv3+) trained to identify keratinocytic structures on HE stains of 13 manually annotated images (4.38 mm^2 epidermis label area, 30.4 mm^2 dermis label area, and 19.8 mm^2 background label area) and tested on ten other images from different patients. Training and test lesions were benign nevi and melanomas not included in the study cohort. A border region that extended 100 μm into dermis from the outlined epidermal boundary was added to account for epidermal melanocytic nests in the superficial dermal region (Fig. 2, Step C2 and Suppl. Fig. 2). Furthermore, this app identified gland structures (a few needed manual correction) in dermis that were excluded from the final Ki67-indexes.

For nuclei identification and classification (Fig. 2, Step C3), three different approaches for DIA apps were developed and tested; 1) red-green-blue thresholds, 2) colour deconvolution thresholds, and 3) AI colour classification. Detailed description of the apps based on the two first approaches can be found in Suppl. Table 1. The AI colour classification app was based on a convolutional neural network (U-net) that was trained on manually corrected nuclei classification labels (33,688 SOX10 labels (class weight: 1), 540 Ki67/SOX10 labels (class weight: 10), 1280 Ki67 labels (class weight: 7.5), and 1.77 mm^2 background label area) on 24 mIHC stained images with varying staining intensities from 19 lesions. The AI app was pre-tested on whole slide images from four other lesions, before applying it to the present study cohort. Train and pre-test lesions were from benign and malignant lesions not included in present study cohort. Postprocessing steps were added to the AI colour classification app to correct for dot-like positivity, overlapping nuclei, deeply blue nuclei, and bluish pigmentation. Additionally, a 1-mm^2 square hot spot was automatically identified by a subsequent app utilizing an object heatmap feature to mark the area with the highest intensity of Ki67/SOX10 double positive labels in a combined region of border and dermis. The nuclei classification app automatically quantified the number of all nuclei classes in the different regions.

2.6.3. Quantification of the Ki67/SOX10-index

The Ki67/SOX10-index was quantified as the number of Ki67/SOX10 double positive nuclei out of all SOX10 positive melanocytic nuclei:

$$Ki67\Big/SOX10\ index = \frac{N_{Ki67\&SOX10dbl.pos.nuclei}}{N_{SOX10monopos.nuclei} + N_{Ki67\&SOX10dbl.pos.nuclei}} \cdot 100\%$$

2.6.4. Quantification of the Ki67-mono-index

The Ki67-mono-index could be calculated based on the results of the Ki67/SOX10 DIA including quantifications of the total number of cell nuclei on the HE image in the overall tumour region defined by the pathologist or in subregions. The Ki67-mono-index was quantified as the number of all Ki67 positive nuclei out of the total number of all nuclei:

$$Ki67mono\ index = \frac{N_{Ki67\ positive\ nuclei}}{N_{All\ nuclei(HE)}} \cdot 100\%$$

2.6.5. Quantification of Ki67/MART1-indexes

The Ki67/MART1-indexes was calculated from the original data from the initial DIA analysis performed previously by Nielsen et al.[30] The index was quantified both as a Ki67/MART1-index similar to the above described Ki67/SOX10-index and, furthermore, as the best performing index in the original study (the combined Ki67/MART1-area-index). The combined Ki67/MART1-area-index was calculated by defining the numerator as the area of all epidermal and dermal Ki67-positive, MART1-verified nuclei. The denominator (reference area) was defined as the total area of epidermis and the area of all MART1 positive cells in dermis[30]:

$$Ki67/MART1\ index = \frac{N_{Ki67\ positive,MART1verified\ nuclei}}{N_{All\ MART1verified\ nuclei}} \cdot 100\%$$

$$Combined\ Ki67/MART1\ areaindex = \frac{Area_{Ki67positive,\ MART1verified\ nuclei}}{Area_{Epidermis} + Area_{Dermal\ MART1verified\ tumour\ cells}} \cdot 100\%$$

2.7. PRAME/SOX10 digital image analysis

The analysis of PRAME/SOX10 was performed using the same DIA steps as describe above (Suppl. Fig. 1 C). In Step C1, the digital image of the PRAME (FastRed)-haematoxylin stain was aligned with the digital image of the SOX10 (DAB)-haematoxylin stain. In Step C2, the manually outlined overall tumour region from the initial HE was transferred to the PRAME slides to ensure comparable analysis. In six cases, an experienced dermatopathologist (TS) manually outlined a new overall tumour region because the tissue appearance differed due to deeper cutting of the original tissue block. The app utilized for outlining the dermo-epidermal boundary in the Ki67/SOX10 DIA was retrained on 13 manually annotated 'ground truth' PRAME(FastRed)-haematoxylin images (benign and malignant lesions not included in study cohort) to fit the PRAME stain. This app similarly included the 100 μm border region.

The nuclei identification and classification (Step C3) were based on Visiopharm's pre-trained Deep Learning (U-net) app. All nuclear structures on the SOX10 (DAB)-haematoxylin image were identified. The app then first classified the nuclei according to their positivity in SOX10 (DAB), and, subsequently, classified the SOX10 positive nuclei according to their positivity in PRAME (FastRed). Detailed information about this app is provided in a previously published paper[35]. A 1 mm^2 square hot spot was additionally identified by an app similar to the Ki67/SOX10 hot spot app.

2.8. Quantification of the PRAME/SOX10-index

The PRAME/SOX10-index was quantified as the number of PRAME/SOX10 double positive nuclei out of all SOX10 positive melanocytic

nuclei:

$$PRAME \Big/ SOX10\ index = \frac{N_{PRAME\&SOX10dbl.pos.\ nuclei}}{N_{All\ SOX10pos.\ nuclei}} \cdot 100\%$$

2.9. PRAME-mono digital image analysis

The analysis of the PRAME-mono stains was performed similar to the PRAME/SOX10 DIA described above, however, the image alignment step was excluded (Suppl. Fig. 1D). Instead, the DIA analysis of the PRAME-mono stain started directly with the region outlining (Suppl. Fig. 1D, Step D1). This was performed utilizing the same app for epidermal border identification as described above for the PRAME/SOX10 analysis. Next, the nuclei identification and classification in the PRAME-mono stains were based on Visiopharm's pre-trained Deep Learning (U-net) application (Suppl. Fig. 1D, Step D2). The nuclear structures were identified on the PRAME(FastRed)-haematoxylin image. The identified nuclei where then classified according to their positivity in PRAME using the same RGB-colour-band feature (contrast of red and green colour levels) with the same threshold as in the PRAME/SOX10 analysis. A postprocessing step was added to exclude large melanin pigment residues based on thresholds of an 'AEC-DAB'-deconvolution feature.

2.10. Quantification of the PRAME-mono-index

The PRAME-mono-index was quantified as the number of all PRAME positive nuclei out of the total number of all nuclei:

$$PRAMEmono\ index = \frac{N_{PRAME\ pos.nuclei}}{N_{PRAME\ neg.nuclei} + N_{PRAME\ pos.nuclei}} \cdot 100\%$$

2.11. Statistics

Data analysis was performed in STATA 17.0 (StataCorp, College Station, TX, USA). A p-value < 0.05 was considered statistically significant, unless otherwise specified. The diagnostic performance of the indexes was evaluated by area under curve (AUC) of receiver operating characteristics (ROC) with Bamber and Hanley confidence intervals for non-malignant versus malignant lesions and compared by tests of equality (algorithm by Delong 1988[44]). Overall difference in medians of WHO-groups and MPATH-Dx V2.0 classes were compared using non-parametric Kruskal Wallis tests. Individual medians were compared using Wilcoxon rank-sum test by the Hierarchical method (benign vs malignant, class I vs IV) and the Bonferroni method (benign vs intermediate, intermediate vs malignant, class I vs II, II vs III, III vs IV). Possible cut-offs for the two best performing indexes, the border Ki67/SOX10-index and the border PRAME-mono-index, were explored by ROC analysis and by visual examination. Based on the data visualized in Suppl. Fig. 3, a Ki67/SOX10-index cut-off of 1.0 % was chosen to define Ki67-positivity in the border region and the dermal region, and a PRAME-mono-index cut-off of 2.5 % was chosen to define PRAME-positivity in the border region.

3. Results

3.1. Cohort characteristics

Patient and tumour characteristics of the cohort divided by WHO-group are listed in Table 1. A total of 156 lesions were included in the study. Four cases were excluded from the Ki67 analysis due to lack of tissue or staining failures (one benign, one intermediate, and two malignant). Nine cases were excluded from the PRAME-mono analysis due to lack of tissue or staining failures (two benign, two intermediate, and five malignant). Additionally, there were seven cases in which the subsequent SOX10 stain failed, leading to a total of 16 cases being excluded from the PRAME/SOX10 analysis (Suppl. Fig. 4).

Table 1
Patient and tumour characteristics by WHO-group.

Feature:	Benign (n = 49)	Intermediate (n = 57)	Malignant (n = 50)	Difference, p-value
Age in years, mean (SD)[a]	38.2 (22.0)	53.3 (21.1)	59.3 (18.0)	P < 0.001
Sex[b]				P = 0.011
Female, no. (%)	30 (61 %)	40 (70 %)	21 (42 %)	
Male, no. (%)	19 (39 %)	17 (30 %)	29 (58 %)	
Thickness in mm, median (95 % CI)	1.11 (0.71;1.43)	0.39 (0.22;0.55)	0.92 (0.78;1.3)	-
Ulceration, no. (%)[b]	0 (0 %)	0 (0 %)	7 (14 %)	P = 0.569

Note: Hypothesis of no difference tested by: a) One-way analysis of variance, Normal distribution checked by QQ-plots, same SD test by Bartlett's test, b) Pearsons chi-squared test. N = 156.

3.2. Ki67/SOX10 digital image analysis classification

Three different approaches for the DIA cell classifier of the Ki67/SOX10 stain were tested. The cell classifier based on AI colour classification performed significantly better than the others both in terms of diagnostic performance (difference in ROC AUC for overall Ki67/SOX10-indexes; p = 0.006) (Suppl. Table 1, Suppl. Fig. 5) and by visual examination of individual cells. Thus, all the following Ki67/SOX10 analyses are based on data by the AI colour classification.

3.3. The Ki67/SOX10 double nuclear staining

Fig. 3A and 3 C display the ROC curves of digitally quantified Ki67-indexes comparing malignant and non-malignant lesions (benign and intermediate). The Ki67/SOX10-index displayed statistically significantly higher AUC than the Ki67-mono-index (p < 0.001). The ROC curves of the Ki67/SOX10-indexes for the different tissue regions (the overall, epidermal, border, dermal, and hot spot region) all displayed AUC above 0.80, with the border region showing the highest (border AUC: 0.87, 95 % CI: 0.81;0.94) (Fig. 3A). The ROC AUC of the Ki67/SOX10-index increased in all regions when the cohort was limited to lesions with a dermal component (border AUC: 0.91, 95 % CI: 0.85;0.96) or to lesions thicker than 0.80 mm (border AUC: 0.97, 95 % CI: 0.93;1.0) (Suppl. Table 2 and Suppl. Fig. 6A and 6C).

Fig. 4 displays the ROC curves for SOX10-based Ki67-indexes compared to MART1-based Ki67-indexes. The Ki67/SOX10-index displayed statistically significant higher AUC than the Ki67/MART1-index when based on the number of cells (p = 0.040). There was no difference between the AUC of the best performing SOX10-based indexes (the Ki67/SOX10-index of the border region) and the best performing MART1-based index from the original study[30] (the combined Ki67/MART1-area-index) when tested on the present study cohort (p = 0.541). One desmoplastic melanoma was excluded from this analysis due to lack of MART1 positivity.

3.4. The PRAME/SOX10 virtual double nuclear staining

The ROC curves of digitally quantified PRAME-indexes are displayed in Figs. 3B and 3D. The AUC of the PRAME-mono-index tended to be higher than the AUC of the PRAME/SOX10-index, however, this was not statistically significant (p = 0.090). Fig. 3D displays the ROC-curves of different tissue regions, in which the PRAME-mono-index of the border region displayed the highest AUC (border AUC: 0.80, 95 % CI: 0.72;0.89). The ROC AUC of the PRAME-mono-indexes increased when the cohort was limited to lesions with a dermal component (border AUC: 0.86, 95 % CI: 0.78;0.94) or to lesions thicker than 0.80 mm (border AUC: 0.92, 95 % CI: 0.85;1.0) (Suppl. Table 2 and Suppl. Figs. 6B and

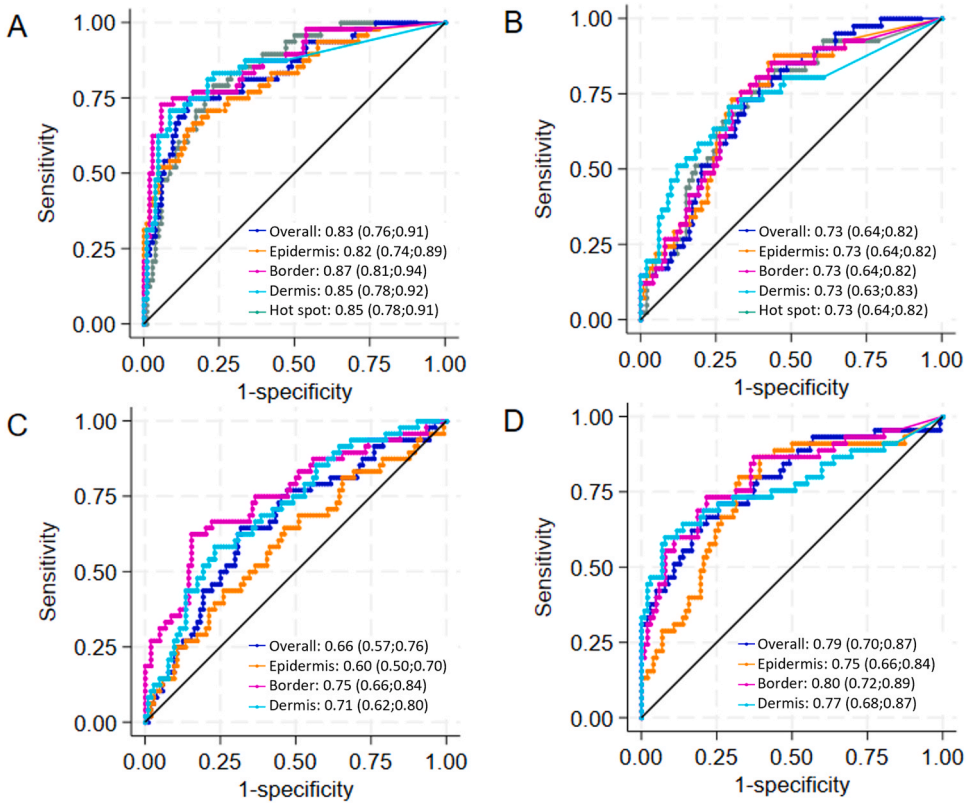

Fig. 3. Diagnostic performance of dividing lesions in malignant and non-malignant (benign and intermediate) in different tissue regions by A) Ki67/SOX10-index (n = 152), B) PRAME/SOX10-index (n = 140), C) Ki67-mono-index (n = 152), and D) PRAME-mono-index (n = 147). The tissue regions are the overall tumor region outlined by the pathologist (overall), epidermis, the dermoepidermal border region (border), and dermis. The regions are listed in the ROC graphs with AUC (95 % CI interval) for each modality.

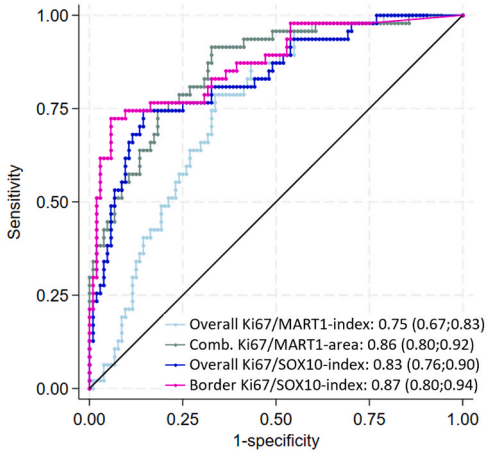

Fig. 4. Comparison of diagnostic performance of Ki67-indexes with either SOX10 or MART1 as melanocytic marker (n = 151). The Ki67/SOX10-index (blue) is compared with the Ki67/MART1-index (light blue), both quantified as number-indexes for the overall tumor region (p = 0.040). The best performing SOX10-based index quantification, the Ki67/SOX10-index of the border region (purple), is compared with the best performing MART1-based index, the combined Ki67/MART1-area-index (gray)(p = 0.541). Both MART1-based index calculations are based on the Ki67/MART1 data from the study by Nielsen et al. [30]. The indexes are listed in the ROC graphs with AUC (95 % CI interval) for each modality.

6D).

3.5. Ki67 and PRAME in WHO-groups and MPATH-Dx V2.0 classes

Fig. 5 displays the Ki67/SOX10-indexes and PRAME-mono-index of different lesion groups ordered by WHO-groups and MPATH-Dx V2.0 classes. The median Ki67/SOX10-index and the median PRAME-mono-index were overall statistically significantly different between benign, intermediate, and malignant melanocytic lesions ($p < 0.001$) (Fig. 5, Suppl. Figs. 7 A and 7 C). The individual difference in medians between the intermediate group and the malignant group was statistically significant both for the Ki67/SOX10-index and for the PRAME-mono-index in all regions ($p < 0.01$) (Fig. 5, Suppl. Table 3). Similarly, the median Ki67/SOX10-index and the median PRAME-mono-index were overall statistically significantly different for the MPATH-Dx V2.0 groups ($p < 0.001$) (Fig. 5, Suppl. Fig. 7D). The individual difference in medians between MPATH-Dx V2.0 group II (high grade) and III (thin melanomas) was not statistically significant for the Ki67/SOX10-index or the PRAME-mono-index. However, the median Ki67/SOX10-index of the border region tended to be higher in group III compared to II (III: 2.2, 95 % CI: 0.62;3.8 vs II: 0.63, 95 % CI: 0.37;1.1, p = 0.019) (Fig. 5, Suppl. Table 3, Suppl. Fig. 7D).

3.6. Combining digitally quantified Ki67- and PRAME-indexes

Fig. 6 displays the combined results of the border Ki67/SOX10-index and the border PRAME-mono-index for each lesion. Twenty-six out of 35 lesions displaying double positivity were melanomas, and 37 out of 45 melanomas were positive for at least one marker (Fig. 6, Suppl. Table 4). Three out of 47 lesions in the WHO-group of benign nevi and six out of 56 lesions in the intermediate group were positive for both markers

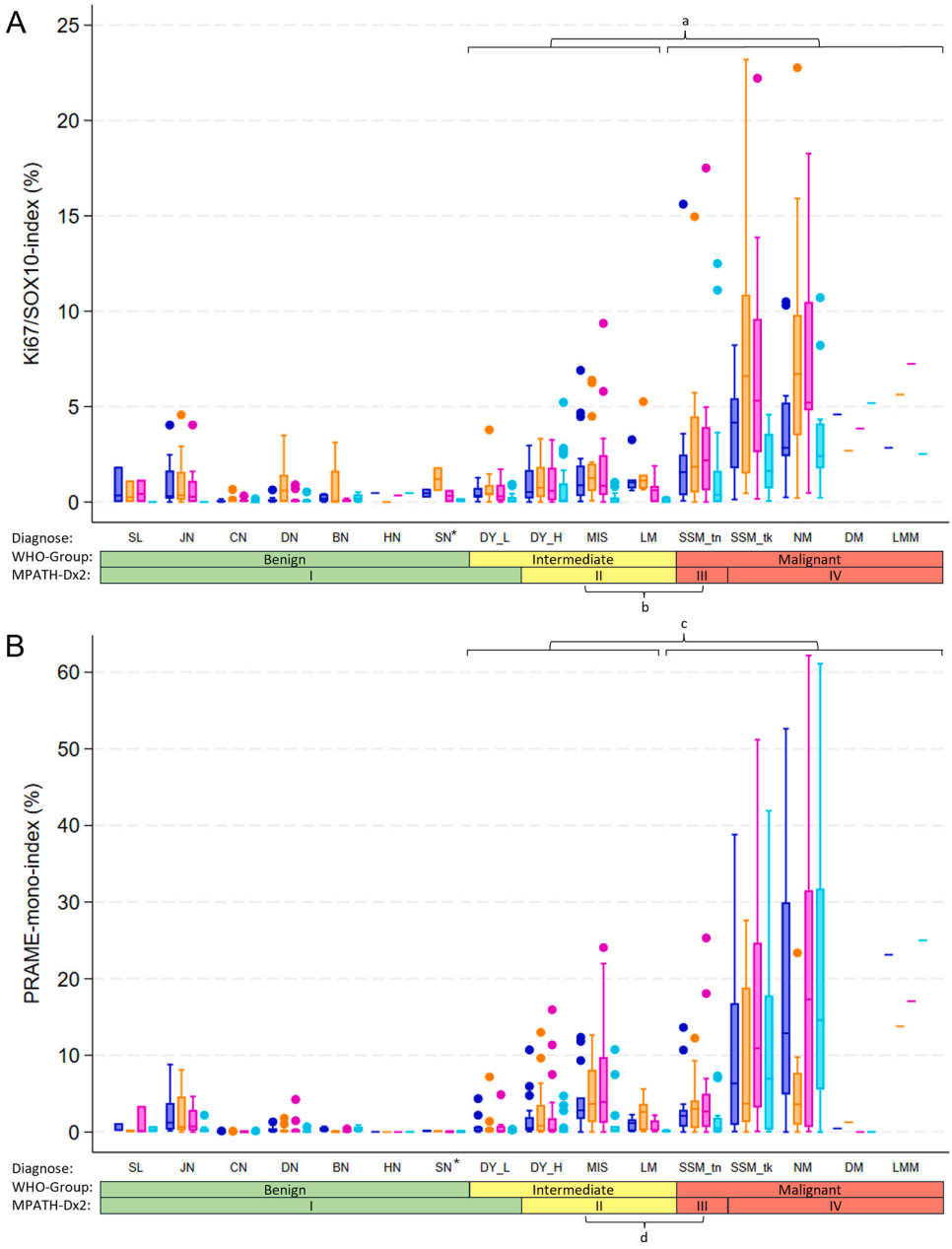

Fig. 5. Boxplot of A) Ki67/SOX10-indexes (n = 152) and B) PRAME-mono-indexes (n = 147) for different tissue regions; overall (blue), epidermis (orange), border (magenta) and dermis (cyan). The indexes are displayed in different diagnostic groups and ordered according to WHO-groups and MPAT-Dx V2.0 classification. * Spitz nevi (SN) are grouped as benign in WHO-group and classified as MPATH-Dx V2.0 class II. a) Statistically significant difference in Ki67/SOX10-index between intermediate and malignant lesions for all tissue regions ($p < 0.001$). b) Difference in Ki67/SOX10-index between MPATH-Dx V2.0 class II and III for the border region with $p = 0.019$. c) Statistically significant difference in PRAME-mono-index between intermediate and malignant lesions for all tissue regions ($p < 0.01$). d) Difference in PRAME-mono-index was not statistically significantly different between MPATH-Dx V2.0 class II and III in any of the regions (Border region: $p = 0.131$). Abbreviations: SL: Lentigo simplex, JN: Junctional nevi (common benign), CN: Combined nevi (common benign), DN: Dermal nevi (common benign), BN: Blue nevi, HN: Halo nevi, SN: Spitz nevi, DY_L: Dysplastic nevi, Low grade, DY_H: Dysplastic nevi, High grade, MIS: Melanoma in situ, LM: Lentigo maligna, SSM_tn: Superficial spreading melanoma, thin (<0.8 mm), SSM_tk: Superficial spreading melanoma, thick (>0.8 mm), NM: Nodular melanoma, DM: Desmoplastic melanoma, LMM: Lentigo maligna melanoma.

(Fig. 6, Suppl. Table 4).

4. Discussion

In this study, we tested the performance of a diagnostic tool utilizing digital quantification of Ki67 and PRAME in a cohort of challenging melanocytic lesions. The results showed that it was possible to accurately quantify Ki67- and PRAME-indexes in melanocytic lesions using DIA, and that a double stain with SOX10 as tumour marker improved the diagnostic performance of Ki67, but not PRAME. Moreover, the findings indicated that the diagnostic value was greatest when assessing the positivity of the epidermal border region, and that the expression of Ki67 and PRAME differed across WHO-groups and MPATH-Dx V2.0 classes. Combining digitally quantified Ki67- and PRAME-indexes in a diagnostic tool reduced the number off misclassified lesions. This tool may thus serve as a useful diagnostic aid in challenging melanocytic lesions by providing accurate, melanocytic cell specific, compartment stratified biomarker indexes with high reproducibility.

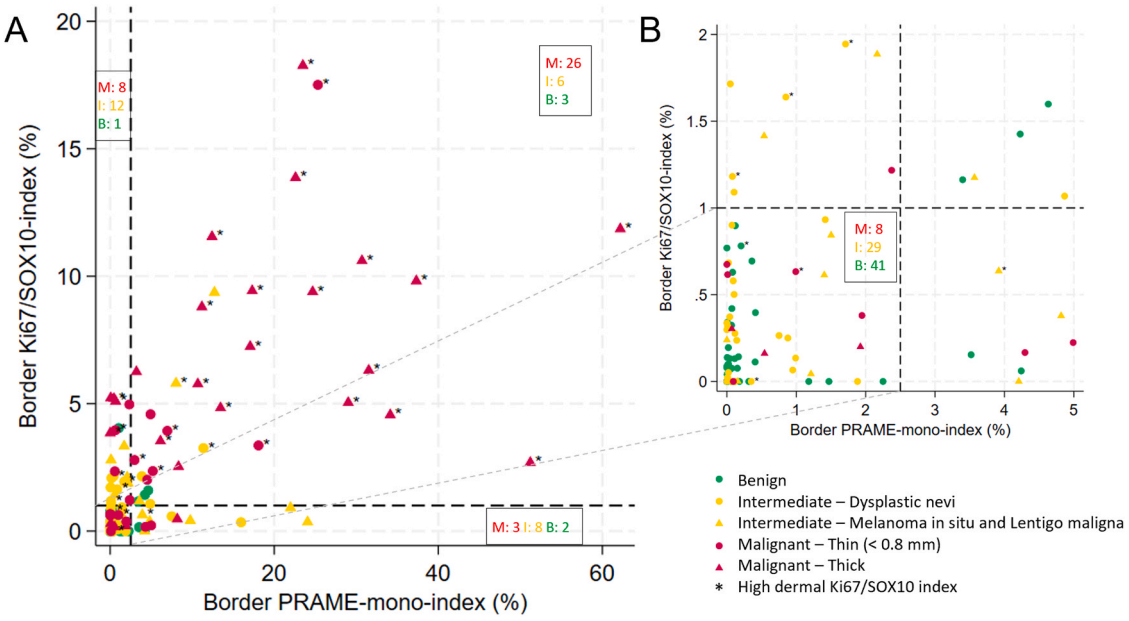

Fig. 6. A) Combination of Ki67 and PRAME indexes. All cases (n = 147) plotted by border Ki67/SOX10-index and border PRAME-mono-index with cutoffs at 1 % and 2.5 %, respectively. Lesions are colored according to WHO groups. Lesions with a high (>1 %) dermal Ki67/SOX10-index are labelled with * . Insets show number of benign (B, green), intermediate (I, yellow) and malignant (M, red) lesions in the different plot-regions. B) Zoom of plot region.

4.1. SOX10 improved the diagnostic performance of Ki67 compared to Ki67 alone

In line with previous literature[26,29–31], we found that combining Ki67 with a melanocytic marker enhanced the diagnostic performance. This underlines that accurate identification of tumour cells is essential when interpreting Ki67 in melanocytic lesions. The present study further included a direct comparison of the proposed nuclear melanocytic marker SOX10, with the previously studied cytoplasmatic melanocytic marker MART1, performed on the same cohort of melanocytic lesions. When comparing the ROC AUC of similarly quantified number-based Ki67-indexes (comparable to clinical manual assessment), SOX10 exhibited a significantly improved diagnostic performance compared to MART1 (Fig. 4). In contrast, there was no difference in AUC when comparing the best performing SOX10-based index (the Ki67/SOX10-index of the border region) with the previously best performing MART1-based index (the combined Ki67/MART1-area-index) [30] tested on the same study cohort. Although, the best-performing algorithms showed very similar diagnostic performance in this study, we believe that this could have been different in a cohort comprising more heavily pigmented and inflamed lesions, given the designated pitfalls of MART1 in Ki67 analysis related to brown pigmentation mimicking DAB stain and lymphocytes overlapping melanocytic cytoplasm. Furthermore, the desmoplastic melanoma in the cohort was excluded from the comparative analysis, as it did not express MART1 and, consequently, could not be quantified using the Ki67/MART1 technique. Utilizing the Ki67/SOX10 method, this desmoplastic melanoma displayed a considerably elevated Ki67 positivity (Overall Ki67/SOX10 index: 4.59 %, Border Ki67/SOX10 index: 3.85 %), underlining the advantage of SOX10 in this particular group of lesions. Therefore, we argue that the Ki67/SOX10-index still poses a considerable improvement for accurate melanocytic cell specific proliferation indexes in challenging melanocytic lesions.

To account for deep epidermal melanocytic nest and to specifically address the superficial part of dermis, which is where the most proliferative activity is commonly observed, we developed an AI-based DIA app to automatically identify the keratinocytic structures in epidermis. This superficial proliferative activity is typically considered less diagnostically significant than deep dermal proliferative activity in melanocytic lesions[5,11]. Nevertheless, our results showed that the Ki67/SOX10-index at the border region displayed the highest AUC, suggesting the potential diagnostic value of this particular region (Fig. 3A). To our knowledge, not many studies have investigated Ki67 specifically in this region. The deep dermal region, profound of the border region, exhibited very low Ki67/SOX10-index values in nearly all benign and intermediate lesions and elevated values in the majority of thick melanomas (Fig. 5A). However, a considerable proportion of thin melanomas exhibited minimal or absent Ki67positivity in the dermal region, despite the majority contained an adequate number of melanocytic cells in the dermal region. These findings align with previous findings by Nielsen et al.[30], and indicate that the presence of Ki67 activity in the deep dermal compartment is a strong indicator of malignancy, though its absence does not exclude malignancy. Overall, these finding implies that the histomorphological location of the Ki67 positivity is of relevance in the diagnostic assessment of melanocytic lesions.

4.1.1. The diagnostic performance of PRAME was not improved by SOX10

Contrary to the Ki67 outcomes, the results showed that the PRAME/SOX10 virtual double nuclear staining did not enhance the diagnostic performance of PRAME. In fact, our analysis revealed that the performance of PRAME as a mono stain tended to be superior to PRAME in combination with SOX10. We consider several potential reasons for this. First of all, we observed that PRAME demonstrates a more qualitative character, in contrast to the more quantitative character of Ki67 positivity. This means that the diagnostic value of PRAME turned out to be primarily dependent on whether significant PRAME positivity was present or not, rather than the specific quantitative amount of PRAME positivity. Thereby the diagnostic performance of PRAME were less dependent on precise tumour cell identification. Secondly, in contrast to Ki67, the risk of 'false-positive' PRAME staining in other cells turned out to be very limited. Apart from melanocytic cells, sebaceous cells were the only cell type in skin tissue that expressed PRAME. These were located in distinct glandular formations that were easily distinguished from melanocytic cells and possible to identify by the DIA app outlining the different regions of the tumour, and they were thus subsequently excluded from the analysis. Instead of enhancing accuracy, the inclusion of SOX10 in the MICSSS PRAME/SOX10 double nuclear stain introduced

technical challenges: 1) We observed a weaker staining intensity compared to routine stains for the PRAME stain, but especially for the SOX10 stain. This may be coursed by the subsequent staining rounds in the MICSSS method used (Suppl. Fig. 1). However, it is also worth considering that the relatively advanced age of the tissue blocks could account for the loss of PRAME positivity, as also observed in a study conducted by Parra et al. in 2023[45]. 2) As the PRAME/SOX10 stain was not a true double nuclear stain like the Ki67/SOX10 stain, but rather a virtual double nuclear stain, it is dependent on the accuracy of the digital alignment of the two separate stains. Although, the two stains were performed on the same tissue slide, it was not always possible to achieve complete digital alignment of all nuclei, causing a possible misclassification of mis-aligned cells.

In the literature, the cut-off for PRAME positivity was initially proposed to be at 75 % positive cells (equal to score 4 +)[27]. However, it has been suggested to lower the cut-off to 50 % (equal to score 3 +), since several studies have found a significant proportion of melanomas only displaying a PRAME expression equal to a score of + 3 [22,45,46]. Recent studies indicate that varied cut-offs may be appropriate for specific types of melanocytic lesions, such as Spitz, acral and mucosal lesions[38,47,48]. However, our study cohort did not include enough of these specific tumour types to perform individual statistical analyses. Our digital PRAME results showed very low percentage values, both when quantified as the PRAME/SOX10-index and as the PRAME-mono-index. Two other studies have used DIA for quantification of PRAME. Rawson et al. quantified number indexes based on immunofluorescent stains of PRAME and SOX10 and reported percentages values lower than the values initially reported for PRAME[33]. Koch et al. quantified PRAME as the number of positive cells per mm^2 area, why the index values were not directly comparable to the manual indexes[33,34]. Generally, studies that employ digital quantification observe lower index values, making it difficult to directly transfer the cut-offs to manual assessment in routine pathology.

4.1.2. Ki67 and PRAME expression differs between WHO-groups and MPATH-Dx V2.0 classes

To our knowledge, the expression of PRAME and Ki67 has not previously been compared between different WHO-groups or between MPATH-Dx V2.0 classes. Our results showed that medians of both Ki67 and PRAME-indexes significantly differed when comparing the overall WHO-groups. Statistically significant differences were also observed when comparing the intermediate and malignant WHO-groups individually (Fig. 5, Suppl. Fig. 7). When looking at the different tumour regions, very little dermal expression of both Ki67 and PRAME was observed in benign and intermediate lesions. This observation suggests that dermal PRAME and Ki67 positivity could serve as a significant indicator of potential malignancy. However, since not all malignant lesions displayed a marked increase in dermal Ki67 and PRAME positivity, the border region turned out to yield the best diagnostic performance. Additionally, we saw that the epidermal PRAME- and Ki67-indexes were elevated in some of the intermediate lesions as melanoma in situ, lentigo maligna, and high-grade dysplastic nevi (Fig. 5). This is in line with reports of increased Ki67 activity in suprabasal (pagetoid) melanocytic cells in melanoma in situ by Hall et al.[49].

The same tendencies were observed when classifying the lesions according to the MPATH-Dx V2.0. Both Ki67 and PRAME significantly differed when comparing the overall classes (Fig. 5, Suppl. Fig. 7). Additionally, the diagnostic performances of both the Ki67/SOX10-indexes and PRAME-indexes were high when assessing only thick lesions (>0.80 mm) corresponding to MPATH-Dx V2.0 class IV melanomas and non-malignant lesions of similar thickness (Suppl. Fig. 7 and Suppl. Table 2). However, when comparing only class II (high-grade) and class III (thin melanoma), only the Ki67-index of the border region seemed to differ, however, only with borderline significance (Fig. 5, Suppl. Table 3, Suppl. Figs. 7B and 7D). In fact, the PRAME-indexes were almost identical between MPATH-Dx V2.0 class II and III. The distinction between melanoma in situ (class II) and thin melanomas (class III) is one of the most challenging tasks with reports of very low accuracy and reproducibility[2,4]. Hence, there remains a need for diagnostic tools to differentiate these cases, as evidenced by reports indicating a higher usage of IHC markers in melanoma in situ compared to invasive melanomas[50,51].

4.1.3. Combining Ki67- and PRAME-indexes lowers numbers of misclassified melanomas

Our results showed that the number of misclassified lesions was reduced when combining Ki67- and PRAME-indexes (Fig. 6, Suppl. Table 4). The approach of combining several diagnostic biomarkers have previously been proposed, however, most of these have assessed the IHC stains manually[20–22]. Rasic et al. reported increased specificity by combing PRAME with HMB45, and Uguen et al. reported reduction of misclassified lesions when combining Ki67, HMB45, and P16[20,21]. The combined use of PRAME and Ki67 have recently been proposed by Mert et al., however, this study did not include a combined analysis of PRAME and Ki67[22]. In our combined analysis, we found that most cases were melanomas when both Ki67- and PRAME-indexes were positive as visualised in the upper quadrant of the graph in Fig. 6A. This corresponds to a high specificity when using combined positivity in both PRAME and Ki67 (Suppl. Table 4). However, this was accompanied by a relatively low sensitivity, since a considerable part of the melanomas only displayed positivity in one of the markers. Conversely, the sensitivity markedly increased when either Ki67 or PRAME positivity was considered, albeit with a corresponding decrease in specificity. However, twenty-six out of 56 lesions in the intermediate group were also positive for at least one marker. Hence, we suggest that positivity in both markers can be considered a robust indicator of potential malignancy, while positivity in only one marker should be viewed as a marker of caution for possible malignancy prompting the pathologist's careful consideration during evaluation.

Although the combined tool increased the sensitivity, eight malignant lesions were still negative in both markers with the chosen threshold of 1.0 % for Ki67 and 2.5 % for PRAME. We reviewed these cases and found that all were almost entirely negative in the PRAME stain. Two of the missed lesions had a prominent benign nevus component, that may have contributed to the low Ki67- and PRAME-indexes by 'diluting' their positivity. Five lesions displayed a very small dermal component in comparison to the initially measured Breslow thickness, suggesting that central parts of the study lesion were missing. These cases highlight the significance of ensuring that the slide accurately represents the lesion and emphasize the importance of integrating ancillary quantitative tools with conventional morphological examination.

4.1.4. Strengths and limitations

A limitation of this study was that it comprised a condensed cohort; hence, it did not reflect the prevalence of lesions in a routine workflow at a clinical pathology department. Accordingly, the sensitivities, specificities, and cut-offs of the study are not directly transferable to a clinical setting. Recent studies have similarly focussed on evaluation of Ki67 in cohorts specifically enriched with challenging lesions, with findings of higher Ki67 expression in melanomas than in ambiguous lesions[22,52]. Although the results of this study showed limited ability to completely discriminate the MPATH-Dx V2.0 classes II (high-grade atypia/MIS) and III (thin melanomas), we still believe that the tool adds valuable insight for the diagnostic assessment of these lesions, since the Ki67/SOX10 index of the border region did tend to differ between these groups ($p = 0.019$). We believe that focussing on the challenging lesions is necessary to develop and evaluate a diagnostic tool because the pathologist possibly will utilize the tool mainly within this subgroup[50,51]. Though, to establish cut-off levels and the predictive values of the diagnostic tool further validation on a larger consecutive cohort is needed.

An additional challenge of focussing on the challenging lesions is that the gold standard diagnosis of these lesions may be difficult to settle. In order to ensure the accuracy of the consensus diagnosis, a thorough re-evaluation was conducted of all the lesions in the study cohort by two experienced dermatopathologists resulting in a consensus diagnosis[30]. This approach has been utilized in other studies of diagnostic performance in melanocytic lesions and has been considered the most optimal in clinical practice[1,4]. Furthermore, we conducted a review of all cases in the national pathology register after 10 years of follow up, to assure that no patients without melanoma had developed metastatic disease.

4.1.5. Clinical implications

During the development of the diagnostic tool described in this paper, our focus was that the workflow of the proposed methods could be practically implemented within a clinical workflow in a modern pathology department. Firstly, the proposed workflow of the Ki67/SOX10 double nuclear stain requires no extra time than a traditional Ki67 mono stain (from day to day). Secondly, the translucent chromogens utilized for the double nuclear stain are about to be tested for clinical use. Thirdly, although the initially tested PRAME/SOX10 virtual double nuclear stain took two days to perform in the laboratory, the final incorporated PRAME-mono stain, that is already performed in routine laboratories, only takes a day. Furthermore, even though the suggested workflow relies on digital assessment and quantification, both stains can still be manually assessed using a conventional microscope. This allows for their utilization in departments that are not yet digitalized.

The novel diagnostic tool proposed in this paper combines traditional HE, multiplex IHC, and DIA, acknowledging the morphology of the standard HE as the primary source of diagnostic information, but supplements it with additional tools as IHC and DIA[18,53]. With this method the pathologist can visualise each single cell both in HE morphology and in mIHC double stains. Furthermore, they receive accurate and reproducible DIA quantifications of biomarkers per cell type and tissue region. These methods could potentially have utility in other cancer types, particularly when accurate and reproducible quantification of histological biomarkers is required in the diagnostic assessment.

5. Conclusion

In conclusion, our study demonstrated that DIA can be effectively utilized to obtain objective quantifications of Ki67 and PRAME. The diagnostic performance was improved by employing the Ki67/SOX10 double nuclear stain for cell-specific quantification of Ki67. In contrast, the diagnostic performance of PRAME was not improved by SOX10. Combining digitally quantified Ki67- and PRAME-indexes reduced the number of misclassified melanomas. Furthermore, we found that Ki67 and PRAME-indexes varied significantly between WHO-groups and MPATH-Dx V2.0 classes. The diagnostic tool proposed in this study may serve as a useful aid in the diagnosis and classification of challenging melanocytic lesions by providing accurate and reproducible quantification of diagnostic biomarkers.

Funding

This work was supported by Harboefonden (Grant number 20128), Denmark, Søster & Verner Lipperts Fond, Denmark, Health Research Foundation of Central Denmark Region (Grant number A3139), Denmark, Dagmar Marshalls Fond, Denmark, and Torben & Alice Frimodts Fond, Denmark.

CRediT authorship contribution statement

Nielsen Patricia Switten: Writing – review & editing, Supervision, Software, Resources, Funding acquisition, Conceptualization. **Georgsen Jeanette Bæhr:** Writing – review & editing, Methodology. **Christensen Kristina Bang:** Writing – review & editing, Methodology. **Wandler Anne:** Writing – review & editing, Validation, Conceptualization. **Lade-Keller Johanne:** Writing – review & editing, Validation, Supervision, Investigation, Conceptualization. **Steiniche Torben:** Writing – review & editing, Supervision, Methodology, Conceptualization. **Brogård Mette Bak:** Writing – original draft, Visualization, Software, Project administration, Methodology, Investigation, Funding acquisition, Formal analysis, Conceptualization.

Declaration of generative AI and AI-assisted technologies in the writing process

During the preparation of this work the authors used *ProWritingAid Anywhere for Windows - Grammarly for Your Desktop* (International House, 36–38 Cornhill, London EC3V 3NG, United Kingdom) in order to review the formulation of single sentences during the review and editing process. After using this tool, the authors reviewed and edited the content as needed and takes full responsibility for the content of the publication.

Declaration of Competing Interest

The authors declare the following financial interests/personal relationships which may be considered as potential competing interests: Mette Bak Brogard reports financial support was provided by Harboe Foundation. Mette Bak Brogard reports financial support was provided by Søster and Verner Lipperts Fond. Patricia Switten Nielsen reports financial support was provided by Health Research Foundation of Central Denmark Region. Patricia Switten Nielsen reports financial support was provided by Dagmar Marshall Fund. Mette Bak Brogard reports financial support was provided by Torben and Alice Frimodts Fund. If there are other authors, they declare that they have no known competing financial interests or personal relationships that could have appeared to influence the work reported in this paper.

Acknowledgements

We would like to extend our sincere gratitude to Jeppe Thagaard, Thomas W. Ramsing, and Henrik Høegh from Visiopharm for their invaluable assistance and expert guidance during the development of the DIA applications for the Ki67/SOX10 analysis.

Appendix A. Supporting information

Supplementary data associated with this article can be found in the online version at doi:10.1016/j.prp.2025.155953.

References

[1] D.E. Elder, M.M. Eguchi, R.L. Barnhill, K.F. Kerr, S.R. Knezevich, M.W. Piepkorn, L. M. Reisch, J.G. Elmore, Diagnostic error, uncertainty, and overdiagnosis in melanoma, Pathology 55 (2023) 206–213, https://doi.org/10.1016/j.pathol.2022.12.345.

[2] R.L. Barnhill, D.E. Elder, M.W. Piepkorn, S.R. Knezevich, L.M. Reisch, M.M. Eguchi, B.C. Bastian, W. Blokx, M. Bosenberg, K.J. Busam, R. Carr, A. Cochran, M.G. Cook, L.M. Duncan, R. Elenitsas, A. de la Fouchardiere, P. Gerami, I. Johansson, J. Ko, G. Landman, A.J. Lazar, L. Lowe, D. Massi, J. Messina, D. Mihic-Probst, D. C. Parker, B. Schmidt, C.R. Shea, R.A. Scolyer, M. Tetzlaff, X. Xu, I. Yeh, A. Zembowicz, J.G. Elmore, Revision of the Melanocytic Pathology Assessment Tool and Hierarchy for Diagnosis Classification Schema for Melanocytic Lesions: A Consensus Statement, JAMA Netw. Open 6 (2023) e2250613, https://doi.org/10.1001/jamanetworkopen.2022.50613.

[3] J.E. Gershenwald, R.A. Scolyer, K.R. Hess, V.K. Sondak, G.V. Long, M.I. Ross, A. J. Lazar, M.B. Faries, J.M. Kirkwood, G.A. McArthur, L.E. Haydu, A.M. M. Eggermont, K.T. Flaherty, C.M. Balch, J.F. Thompson, P. for members of the American Joint Committee on Cancer Melanoma Expert, D. the International Melanoma, P. Discovery, Melanoma staging: Evidence-based changes in the American Joint Committee on Cancer eighth edition cancer staging manual, CA Cancer J. Clin. 67 (2017) 472–492, https://doi.org/10.3322/caac.21409.

[4] J.G. Elmore, R.L. Barnhill, D.E. Elder, G.M. Longton, M.S. Pepe, L.M. Reisch, P. A. Carney, L.J. Titus, H.D. Nelson, T. Onega, A.N.A. Tosteson, M.A. Weinstock, S.

R. Knezevich, M.W. Piepkorn, Pathologists' diagnosis of invasive melanoma and melanocytic proliferations: observer accuracy and reproducibility study, BMJ 357 (2017) j2813, https://doi.org/10.1136/bmj.j2813.
[5] D. Ivan, V.G. Prieto, Use of immunohistochemistry in the diagnosis of melanocytic lesions: applications and pitfalls, Future Oncol. 6 (2010) 1163–1175, https://doi.org/10.2217/fon.10.81.
[6] M.L. Wilson, Histopathologic and Molecular Diagnosis of Melanoma, Clin. Plast. Surg. 48 (2021) 587–598, https://doi.org/10.1016/j.cps.2021.05.003.
[7] D.E. Elder, B.C. Bastian, I.A. Cree, D. Massi, R.A. Scolyer, The 2018 World Health Organization Classification of Cutaneous, Mucosal, and Uveal Melanoma: Detailed Analysis of 9 Distinct Subtypes Defined by Their Evolutionary Pathway, Arch. Pathol. Lab Med 144 (2020) 500–522, https://doi.org/10.5858/arpa.2019-0561-RA.
[8] M.W. Piepkorn, R.L. Barnhill, D.E. Elder, S.R. Knezevich, P.A. Carney, L.M. Reisch, J.G. Elmore, The MPATH-Dx reporting schema for melanocytic proliferations and melanoma, J. Am. Acad. Dermatol. 70 (2014) 131–141, https://doi.org/10.1016/j.jaad.2013.07.027.
[9] S.J. Ohsie, G.P. Sarantopoulos, A.J. Cochran, S.W. Binder, Immunohistochemical characteristics of melanoma, J. Cutan. Pathol. 35 (2008) 433–444, https://doi.org/10.1111/j.1600-0560.2007.00891.x.
[10] L.E. Davis, S.C. Shalin, A.J. Tackett, Current state of melanoma diagnosis and treatment, Cancer Biol. Ther. 20 (2019) 1366–1379, https://doi.org/10.1080/15384047.2019.1640032.
[11] C. Torres-Cabala, E. Li-Ning-Tapia, W.J. Hwu, Pathology-based Biomarkers Useful for Clinical Decisions in Melanoma, Arch. Med Res 51 (2020) 827–838, https://doi.org/10.1016/j.arcmed.2020.09.008.
[12] C. Lezcano, A.A. Jungbluth, K.J. Busam, PRAME Immunohistochemistry as an Ancillary Test for the Assessment of Melanocytic Lesions, Surg. Pathol. Clin. 14 (2021) 165–175, https://doi.org/10.1016/j.path.2021.01.001.
[13] M.D. Reid, P. Bagci, N. Ohike, B. Saka, I. Erbarut Seven, N. Dursun, S. Balci, H. Gucer, K.T. Jang, T. Tajiri, O. Basturk, S.Y. Kong, M. Goodman, G. Akkas, V. Adsay, Calculation of the Ki67 index in pancreatic neuroendocrine tumors: a comparative analysis of four counting methodologies, Mod. Pathol. 28 (2015) 686–694, https://doi.org/10.1038/modpathol.2014.156.
[14] N.S. Vyas, A. Charifa, G.T. Desman, M. Goldberg, R. Singh, R.G. Phelps, J. M. McNiff, Observational Study Examining the Diagnostic Practice of Ki67 Staining for Melanocytic Lesions, Am. J. Derm. 41 (2019) 488–491, https://doi.org/10.1097/DAD.0000000000001379.
[15] R. Riber-Hansen, B. Vainer, T. Steiniche, Digital image analysis: a review of reproducibility, stability and basic requirements for optimal results, APMIS 120 (2012) 276–289, https://doi.org/10.1111/j.1600-0463.2011.02854.x.
[16] B.J. Williams, D. Jayewardene, D. Treanor, Digital immunohistochemistry implementation, training and validation: experience and technical notes from a large clinical laboratory, J. Clin. Pathol. 72 (2019) 373–378, https://doi.org/10.1136/jclinpath-2018-205628.
[17] B.J. Williams, D. Bottoms, D. Treanor, Future-proofing pathology: the case for clinical adoption of digital pathology, J. Clin. Pathol. 70 (2017) 1010–1018, https://doi.org/10.1136/jclinpath-2017-204644.
[18] F. Gibilisco, F. Fraggetta, B.J. Williams, A commemoration of the "digital" side of Juan Rosai: a junior's perspective of the legacy of an all-round pathologist, Pathologica 113 (2021) 305–306, https://doi.org/10.32074/1591-951X-444.
[19] A. Saleem, S. Narala, S.S. Raghavan, Immunohistochemistry in melanocytic lesions: Updates with a practical review for pathologists, Semin Diagn. Pathol. 39 (2022) 239–247, https://doi.org/10.1053/j.semdp.2021.12.003.
[20] D. Rasic, N. Korsgaard, N. Marcussen, E.M. Precht Jensen, Diagnostic utility of combining PRAME and HMB-45 stains in primary melanocytic tumors, Ann. Diagn. Pathol. 67 (2023) 152211, https://doi.org/10.1016/j.anndiagpath.2023.152211.
[21] A. Uguen, M. Talagas, S. Costa, S. Duigou, S. Bouvier, M. De Braekeleer, P. Marcorelles, A p16-Ki-67-HMB45 immunohistochemistry scoring system as an ancillary diagnostic tool in the diagnosis of melanoma, Diagn. Pathol. 10 (2015) 195, https://doi.org/10.1186/s13000-015-0431-9.
[22] M. Mert, O. Bozdogan, N. Bozdogan, M. Gamsizkan, M. Safali, PRAME and Historical Immunohistochemical Antibodies Ki-67, P16, and HMB-45 in Ambiguous Melanocytic Tumors, Am. J. Derm. 46 (2024) 653–662, https://doi.org/10.1097/DAD.0000000000002768.
[23] R.G. Ladstein, I.M. Bachmann, O. Straume, L.A. Akslen, Ki-67 expression is superior to mitotic count and novel proliferation markers PHH3, MCM4 and mitosin as a prognostic factor in thick cutaneous melanoma, BMC Cancer 10 (2010) 140, https://doi.org/10.1186/1471-2407-10-140.
[24] T. Scholzen, J. Gerdes, The Ki-67 protein: from the known and the unknown, J. Cell Physiol. 182 (2000) 311–322, https://doi.org/10.1002/(SICI)1097-4652(200003)182:3< 311::AID-JCP1> 3.0.CO;2-9.
[25] P. Rudolph, C. Schubert, B. Schubert, R. Parwaresch, Proliferation marker Ki-S5 as a diagnostic tool in melanocytic lesions, J. Am. Acad. Dermatol. 37 (1997) 169–178, https://doi.org/10.1016/s0190-9622(97)80121-1.
[26] P.S. Nielsen, R. Riber-Hansen, T. Steiniche, Immunohistochemical double stains against Ki67/MART1 and HMB45/MITF: promising diagnostic tools in melanocytic lesions, Am. J. Derm. 33 (2011) 361–370, https://doi.org/10.1097/DAD.0b013e3182120173.
[27] C. Lezcano, A.A. Jungbluth, K.S. Nehal, T.J. Hollmann, K.J. Busam, PRAME Expression in Melanocytic Tumors, Am. J. Surg. Pathol. 42 (2018) 1456–1465, https://doi.org/10.1097/PAS.0000000000001134.
[28] C. Lezcano, A.A. Jungbluth, K.J. Busam, Immunohistochemistry for PRAME in Dermatopathology, Am. J. Derm. 45 (2023) 733–747, https://doi.org/10.1097/DAD.0000000000002440.
[29] P.S. Nielsen, R. Riber-Hansen, J. Raundahl, T. Steiniche, Automated quantification of MART1-verified Ki67 indices by digital image analysis in melanocytic lesions, Arch. Pathol. Lab Med 136 (2012) 627–634, https://doi.org/10.5858/arpa.2011-0360-OA.
[30] P.S. Nielsen, E. Spaun, R. Riber-Hansen, T. Steiniche, Automated quantification of MART1-verified Ki-67 indices: useful diagnostic aid in melanocytic lesions, Hum. Pathol. 45 (2014) 1153–1161, https://doi.org/10.1016/j.humpath.2014.01.009.
[31] A. Wandler, E. Spaun, T. Steiniche, P.S. Nielsen, Automated quantification of Ki67/MART1 stains may prevent false-negative melanoma diagnoses, J. Cutan. Pathol. 43 (2016) 956–962, https://doi.org/10.1111/cup.12778.
[32] M.B. Brogard, P.S. Nielsen, K.B. Christensen, J.B. Georgsen, A. Wandler, J. Lade-Keller, T. Steiniche, Immunohistochemical double nuclear staining for cell-specific automated quantification of the proliferation index - A promising diagnostic aid for melanocytic lesions, Pathol. Res Pr. 255 (2024) 155177, https://doi.org/10.1016/j.prp.2024.155177.
[33] R.V. Rawson, E.R. Shteinman, S. Ansar, I.A. Vergara, J.F. Thompson, G.V. Long, R. A. Scolyer, J.S. Wilmott, Diagnostic utility of PRAME, p53 and 5-hmC immunostaining for distinguishing melanomas from naevi, neurofibromas, scars and other histological mimics, Pathology 54 (2022) 863–873, https://doi.org/10.1016/j.pathol.2022.05.012.
[34] E.A.T. Koch, M. Erdmann, C. Berking, F. Kiesewetter, R. Kramer, S. Schliep, M. V. Heppt, Standardized Computer-Assisted Analysis of PRAME Immunoreactivity in Dysplastic Nevi and Superficial Spreading Melanomas, Int J. Mol. Sci. 24 (2023), https://doi.org/10.3390/ijms24076388.
[35] J. Enevoldsen, M.B. Brogard, J. Lade-Keller, K.B. Christensen, J.B. Georgsen, P. S. Nielsen, T. Steiniche, Digital quantification of PRAME for distinguishing melanoma from nevi compared to manual assessment, Pathol. Res Pr. 262 (2024) 155543, https://doi.org/10.1016/j.prp.2024.155543.
[36] C. Lezcano, M. Pulitzer, A.P. Moy, T.J. Hollmann, A.A. Jungbluth, K.J. Busam, Immunohistochemistry for PRAME in the Distinction of Nodal Nevi From Metastatic Melanoma, Am. J. Surg. Pathol. 44 (2020) 503–508, https://doi.org/10.1097/PAS.0000000000001393.
[37] M. Grillini, C. Ricci, V. Pino, S. Pedrini, M. Fiorentino, B. Corti, HMB45/PRAME, a Novel Double Staining for the Diagnosis of Melanocytic Neoplasms: Technical Aspects, Results, and Comparison With Other Commercially Available Staining (PRAME and Melan A/PRAME), Appl. Immunohistochem. Mol. Morphol. 30 (2022) 14–18, https://doi.org/10.1097/PAI.0000000000000972.
[38] C. Ricci, M.V. Altavilla, B. Corti, E. Pasquini, L. Presutti, A.M. Baietti, L. Amorosa, T. Balbi, C. Baldovini, F. Ambrosi, M. Grillini, A. D'Errico, M. Fiorentino, M. P. Foschini, PRAME Expression in Mucosal Melanoma of the Head and Neck Region, Am. J. Surg. Pathol. 47 (2023) 599–610, https://doi.org/10.1097/PAS.0000000000002032.
[39] C. Ricci, E. Dika, F. Ambrosi, M. Lambertini, G. Veronesi, C. Barbara, Cutaneous Melanomas: A Single Center Experience on the Usage of Immunohistochemistry Applied for the Diagnosis, Int J. Mol. Sci. 23 (2022), https://doi.org/10.3390/ijms23115911.
[40] D. Tacha, W. Qi, S. Ra, R. Bremer, C. Yu, J. Chu, L. Hoang, B. Robbins, A newly developed mouse monoclonal SOX10 antibody is a highly sensitive and specific marker for malignant melanoma, including spindle cell and desmoplastic melanomas, Arch. Pathol. Lab Med 139 (2015) 530–536, https://doi.org/10.5858/arpa.2014-0077-OA.
[41] J. Shin, J.G. Vincent, J.D. Cuda, H. Xu, S. Kang, J. Kim, J.M. Taube, Sox10 is expressed in primary melanocytic neoplasms of various histologies but not in fibrohistiocytic proliferations and histiocytoses, J. Am. Acad. Dermatol. 67 (2012) 717–726, https://doi.org/10.1016/j.jaad.2011.12.035.
[42] K.J. Busam, Y.T. Chen, L.J. Old, E. Stockert, K. Iversen, K.A. Coplan, J. Rosai, R. L. Barnhill, A.A. Jungbluth, Expression of melan-A (MART1) in benign melanocytic nevi and primary cutaneous malignant melanoma, Am. J. Surg. Pathol. 22 (1998) 976–982, https://doi.org/10.1097/00000478-199808000-00007.
[43] N.G. Ordonez, Value of melanocytic-associated immunohistochemical markers in the diagnosis of malignant melanoma: a review and update, Hum. Pathol. 45 (2014) 191–205, https://doi.org/10.1016/j.humpath.2013.02.007.
[44] E.R. DeLong, D.M. DeLong, D.L. Clarke-Pearson, Comparing the areas under two or more correlated receiver operating characteristic curves: a nonparametric approach, Biometrics 44 (1988) 837–845.
[45] O. Parra, W. Ma, Z. Li, B.N. Coffing, K. Linos, R.E. LeBlanc, S. Momtahen, A. Sriharan, J.M. Cloutier, W.A. Wells, S. Yan, PRAME expression in cutaneous melanoma does not correlate with disease-specific survival, J. Cutan. Pathol. 50 (2023) 903–912, https://doi.org/10.1111/cup.14495.
[46] I. Zboras, L. Ungureanu, S. Senila, B. Petrushev, P. Zamfir, D. Crisan, F.A. Zaharie, S.C. Vesa, R. Cosgarea, PRAME Immunohistochemistry in Thin Melanomas Compared to Melanocytic Nevi, Diagn. (Basel) 14 (2024), https://doi.org/10.3390/diagnostics14182015.
[47] M. Kunc, N. Zemierowska, F. Skowronek, W. Biernat, Diagnostic test accuracy meta-analysis of PRAME in distinguishing primary cutaneous melanomas from benign melanocytic lesions, Histopathology 83 (2023) 3–14, https://doi.org/10.1111/his.14904.
[48] S.S. Raghavan, J.Y. Wang, S. Kwok, K.E. Rieger, R.A. Novoa, R.A. Brown, PRAME expression in melanocytic proliferations with intermediate histopathologic or spitzoid features, J. Cutan. Pathol. 47 (2020) 1123–1131, https://doi.org/10.1111/cup.13818.
[49] B.J. Hall, P.E. LeBoit, Suprabasal spread of melanocytes in dysplastic nevi and melanoma in situ: Ki-67-labeling rate of junctional melanocytes and suprabasal cells may be a helpful clue to the diagnosis, Am. J. Surg. Pathol. 38 (2014) 1111–1117, https://doi.org/10.1097/PAS.0000000000000224.

[50] T.C. Chen, M.G. Hitchcock, Rate of Immunohistochemistry Utilization in the Diagnosis of Cutaneous Melanocytic Lesions, Am. J. Derm. 43 (2021) e146–e148, https://doi.org/10.1097/DAD.0000000000001946.
[51] M.S. Dinehart, S.M. Dinehart, S. Sukpraprut-Braaten, W.A. High, Immunohistochemistry utilization in the diagnosis of melanoma, J. Cutan. Pathol. 47 (2020) 446–450, https://doi.org/10.1111/cup.13648.
[52] R.N. Al-Rohil, J.L. Curry, C.A. Torres-Cabala, P. Nagarajan, D. Ivan, P.P. Aung, G. F. Lyons, R.L. Bassett, V.G. Prieto, M.T. Tetzlaff, Proliferation indices correlate with diagnosis and metastasis in diagnostically challenging melanocytic tumors, Hum. Pathol. 53 (2016) 73–81, https://doi.org/10.1016/j.humpath.2016.02.019.
[53] J. Rosai, Why microscopy will remain a cornerstone of surgical pathology, Lab Invest 87 (2007) 403–408, https://doi.org/10.1038/labinvest.3700551.